Reconstructing Ancient Egyptian Tombs

Hany Farid

Dartmouth College, Hanover NH, 03755, USA

Summary. From the pyramids of Giza to the tombs of Thebes (modern Luxor), ancient Egypt's glorious history has produced remarkable architecture. Sadly, the nearly four million yearly tourists have taken a heavy toll on many of these ancient structures. Of particular concern are many of the tombs located opposite to Luxor on the western bank of the Nile. Digital reconstruction of these tombs has the potential to help document and preserve these important historical structures. Photographing and reconstruction of these tombs poses new and unique problems that this paper begins to address. Techniques for removing image distortions, recovering 3-D shape, and correcting for lighting imbalances are discussed. A complete reconstruction of the tomb of Sennedjem is shown.

1 Introduction

Approximately 5,000 years ago, Narmer unified Upper and Lower Egypt creating what is arguably one of the greatest civilizations of all time. From the pyramids of Giza to the tombs of Thebes, Egypt's glorious history is enjoyed by nearly four million tourists each year. While the tourism trade bolsters Egypt's economy, it has taken a heavy toll on many of its ancient monuments. Of particular concern are many of the Theban tombs on the western bank of the Nile, opposite modern Luxor. The delicate and vibrant colors found in the tomb paintings have survived for many millennia, but have recently seen significant deterioration due in part to the large number of visitors. Digital reconstruction of these tombs has the potential to help document and preserve these important historical structures while increasing general knowledge and interest (e.g.,virtual museums). Reconstruction of these structures from photographs poses new and unique problems that this paper begins to address.

We have concentrated our initial efforts on the smaller tombs of artisans in Deir el Medina in western Thebes. These were the people who worked on the royal tombs in the Valley of the Kings, located about a kilometer away. In 1886 when what is now designated tomb number 1 was discovered by Maspero [6] in the Deir el Medina area, it proved to be one of those rare occasions because it was still intact having escaped being plundered in antiquity, as was the fate of most royal and private tombs. Tomb number 1

6211 Sudikoff Laboratory, Department of Computer Science, Dartmouth College, Hanover, NH 03755. **tel:** 603.646.2761, **fax:** 603.646.1672, **email:** farid@cs.dartmouth.edu.

belonged to Sennedjem, who shared his "house of eternity" with his wife Iynefer, their children, and grandchildren where they have remained together in this tiny space, undisturbed for over three millennia.

A wireframe rendering of Sennedjem's burial chamber[1] is depicted in Fig. 1. Shown in Fig. 2 are a pair of photographs taken from each end of the chamber. The burial chamber, measuring 5.12 m by 2.61 m with its vaulted ceiling of 2.40 m, is completely decorated. Nearly any photograph of this small room will contain significant distortions due to the curved ceiling, the inherent effects of perspective projection, and the wide-angle lens required to obtain a reasonable field of view. For example, shown in Fig. 3 (top) are a pair of photographs taken from neighboring panels on the curved ceiling. Given the small size of this room, these distortions are impossible to avoid. In the presence of these distortions, it is equally impossible to create a single large-scale seamless mosaic. This paper first describes an image-based technique for removing these distortions. Combined with a simple technique for recovering the 3-D shape, we then construct fully decorated virtual tombs. While not employed in the results presented here, we also propose a technique for automatically correcting for the lighting imbalances that are typical of flash photographs. We hope to incorporate this technique in future reconstructions.

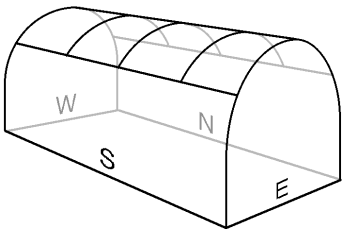

Fig. 1. Sennedjem's burial chamber.

2 Image Distortions

Consider again the pair of images in the top row of Fig. 3. These images were clearly intended to be rectangular in shape. However due to the curved ceiling these images contain significant distortions. Note that these panels neighbor each other on the chamber ceiling. That is, the right-most hieroglyph strip in the left image is the same as the left-most strip in the right image. Our goal is to seamlessly join these images, thus requiring the removal of these distortions. If we assume that the vertical and horizontal hieroglyph strips should be parallel, then these strips provide a convenient landmark for estimating the distortions. Shown in Fig. 3 (top) are 30 points evenly spaced along the outer portion of the panel. These points are determined in a two step process. First, a small number of points (more than four) are manually selected anywhere along a horizontal/vertical portion of the hieroglyph strip that bounds the panel, making sure to choose the two points at either end of the strip. A fourth-order polynomial curve is then fit to these points, from which the equally spaced points are generated. This process is repeated for

[1] Sennedjem's entire tomb consists of several rooms and passageways. The burial chamber is the final room in which Sennedjem was laid to rest.

Fig. 2. The burial chamber of Sennedjem as viewed from each end.

Fig. 3. Shown are images from the curved ceiling before (top) and after (bottom) the removal of distortions.

each side of the panel. Also shown in the same figure is the desired position of these 30 points, automatically chosen to be an equivalent number of equally spaced points along parallel horizontal/vertical lines passing through the average position of the specified distorted contour. By choosing these equally spaced points in the image we are ignoring the surface geometry. As a result, a slight non-uniform compression is introduced in the resulting undistorted image. This effect seems to be qualitatively small.

Clearly, an affine model is insufficient to fully characterize these distortions. Higher-order polynomials offer a natural extension and were employed here. We have found empirically that a third-order polynomial model is sufficient to capture the distortions, while avoiding the instabilities of much higher-order polynomials. The third-order model takes the form:

$$x_u = \alpha_1 x_d^3 + \alpha_2 y_d^3 + \alpha_3 x_d^2 y_d + \alpha_4 x_d y_d^2 + \alpha_5 x_d^2 + \alpha_6 y_d^2 + \alpha_7 x_d y_d + \alpha_8 x_d + \alpha_9 y_d + \alpha_{10}, \quad (1)$$

and

$$y_u = \beta_1 x_d^3 + \beta_2 y_d^3 + \beta_3 x_d^2 y_d + \beta_4 x_d y_d^2 + \beta_5 x_d^2 + \beta_6 y_d^2 + \beta_7 x_d y_d + \beta_8 x_d + \beta_9 y_d + \beta_{10}, \quad (2)$$

where x_d, y_d are the spatial coordinates of the initial distorted points, and x_u, y_u are the coordinates of the desired undistorted points. Our goal is to determine a fixed set of scalar coefficients $\alpha_1, ..., \alpha_{10}$ and $\beta_1, ..., \beta_{10}$ that maps all the specified points from their initial to their desired positions. The coefficients are determined by first combining all the constraints into a single system of linear equations:

$$\begin{pmatrix} x_{u_1} & y_{u_1} \\ x_{u_2} & y_{u_2} \\ \vdots & \vdots \\ x_{u_n} & y_{u_n} \end{pmatrix} = \begin{pmatrix} x_{d_1}^3 & y_{d_1}^3 & \dots & x_{d_1} & y_{d_1} & 1 \\ x_{d_2}^3 & y_{d_2}^3 & \dots & x_{d_2} & y_{d_2} & 1 \\ \vdots & & \ddots & & \vdots & \\ x_{d_n}^3 & y_{d_n}^3 & \dots & x_{d_n} & y_{d_n} & 1 \end{pmatrix} \begin{pmatrix} \alpha_1 & \beta_1 \\ \alpha_2 & \beta_2 \\ \vdots & \vdots \\ \alpha_8 & \beta_8 \\ \alpha_9 & \beta_9 \\ \alpha_{10} & \beta_{10} \end{pmatrix}, \quad (3)$$

which is denoted more compactly as $X = MB$. The scalar coefficients B that best satisfy (in a least-squares sense) these constraints are determined by solving this over-constrained system ($n > 10$) of linear equations using standard least-squares estimation given by:

$$B = (M^t M)^{-1} M^t X, \quad (4)$$

where M^t denotes matrix transpose, and M^{-1} denotes matrix inverse. Using this solution and the assumed mapping of Equations (1) and (2), the desired undistorted position of every point in the initial distorted image can be easily determined. This mapping is then used to re-render the initial image onto the undistorted sampling lattice, Fig. 3 (bottom). Note that the removal of distortions is purely image-based, no knowledge of the 3-D structure, camera pose or intrinsic camera parameters is required. Once the distortions are removed, the images can be brought into alignment with standard affine registration techniques (e.g., [4,9,8]). Note that this affine registration will correct for any errors in the aspect ratio given a properly scaled reference image (see Section 3).

3 Lighting

In addition to the distortions described above, the photographing of Egyptian tombs poses other challenges. The tombs are often poorly lit making it necessary to photograph with a flash, leading to non-uniformities in the lighting. A main contributor to these non-uniformities is the (approximately) quadratic falloff of light intensity as a function of distance. As a result, when photographing, for example, a planar surface, the center of the image can be significantly brighter than the corners. The removal of these variations is critical to the creation of a seamless image mosaic.

Shown in Fig. 4 are the results of manually adjusting for lighting and color imbalances. Note in particular how the darkened corners have been corrected.

Fig. 4. Shown are images with distortions removed before (top) and after (bottom) manual lighting and color adjustments.

In addition, for aesthetic reasons, we identified and digitally removed several modern-day blemishes in background areas. These manipulations were all performed in Photoshop. In future reconstructions, we propose a more automated process that employs a pair of photographs taken with the flash in different positions. Outlined below is a technique for estimating distance, and hence the amount of light attenuation, from such a pair of images. This idea was first proposed by Jarvis in [5], but seems not to have been further explored in the Computer Vision community.

We begin by modeling the flash as a point light source with a quadratic falloff in intensity. For each point X, Y, Z, in the world (and corresponding (x, y) in the image), we denote $L(X, Y, Z)$ as the amount of unattenuated light from the flash reaching the surface, and $R(X, Y, Z)$ as the reflectance function of the surface. An image is then expressed as the product of the reflectance and lighting functions, where the intensity of the light is modulated by the square of the distance to the surface:

$$I_1(x, y) = \frac{L(X, Y, Z) \cdot R(X, Y, Z)}{(X - X_1)^2 + (Y - Y_1)^2 + (Z - Z_1)^2}, \tag{5}$$

where X_1, Y_1, Z_1 denotes the displacement of the flash relative to the camera's nodal point. An additional image taken with no flash can be subtracted from $I_1(\cdot)$ to remove contributions of ambient light. A second image with the flash

in a different position is given by:

$$I_2(x,y) = \frac{L(X,Y,Z) \cdot R(X,Y,Z)}{(X-X_2)^2 + (Y-Y_2)^2 + (Z-Z_2)^2}. \tag{6}$$

Taking the ratio of these images cancels the lighting and reflectance terms. After a few algebraic manipulations, this ratio can be expressed as:

$$\begin{aligned} Z^2 \left[(I_1 X^2 + I_1 Y^2 + I_1) - (I_2 X^2 + I_2 Y^2 + I_2) \right] + \\ Z \left[-2I_1(X_1 X + Y_1 Y + Z_1) + 2I_2(X_2 X + Y_2 Y + Z_2) \right] + \\ \left[I_1(X_1^2 + Y_1^2 Z_1^2) - I_2(X_2^2 + Y_2^2 Z_2^2) \right] = 0 \end{aligned} \tag{7}$$

where $X = x/f$ and $Y = y/f$, and f is the focal length. This equation holds for each point x, y in the image, but for notational convenience the image's spatial parameters are dropped. Note that this easily solved equation is quadratic in a single unknown, the distance Z at each point in the image. Correcting for the light falloff is then a simple matter of multiplying one of the original images by the square of the estimated distance. In addition, variations in brightness due to the angle of the surface relative to the flash can be corrected by considering the spatial derivatives of the recovered distance.

This technique was not applied in the results shown here as the photographs used were taken over a decade ago, and the pair of flash images were simply not available. Nevertheless we propose to use this technique in future reconstructions as it should be well suited for the short-range flash[2] photographs required inside the tombs.

4 Geometry

The relatively simple structure of many ancient Egyptian tombs lends itself to a straight-forward technique for recovering their 3-D shape. Many structures are rectangular at the base with a curved ceiling. Since these structures have been thoroughly studied, the dimensions (length, width, height) are readily available. What remains to be determined is the curvature of the ceiling. This can be determined from a frontal-parallel view of either end of the structure. For example, shown in Fig. 2 are views of Sennedjem's burial chamber as seen from each end. Note that the curvature of the ceiling can be easily determined by simply tracing the contour of one or both end walls. This process can be semi-automated by first selecting a number of points along the contour of each end wall. For each wall, a higher-order polynomial curve is fit to these points, from which a dense

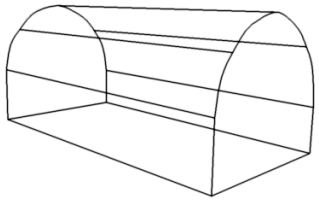

Fig. 5. 3-D reconstruction of Sennedjem's burial chamber (shown in the same orientation as Fig. 1).

[2] Inorganic pigments were used to decorate ancient Egyptian tombs and temples. Unlike dyes, these pigments are very stable and would thus not be adversely affected by flash photography.

sampling of points along each contour can be easily computed. In practice we find given a reasonably dense sampling of points along the contour, as high as a tenth-order polynomial can be used. The final 3-D structure is then determined by directly outputting the shape of the contour in a format readable by a VRML (Virtual Reality Modeling Language) viewer. Shown in Fig. 5 is a wireframe rendering of the recovered 3-D structure of Sennedjem's burial chamber. The curvature was determined as described above, and the proportions were determined from published measurements [1].

5 Reconstructing Sennedjem's Burial Chamber

Shown in Fig. 6 are sixteen photographs that provide full coverage of Sennedjem's burial chamber. These images were digitally scanned at 2700 dpi from 35mm slides. To reduce the demands on memory, each image (3894×2592 pixels) was subsampled by a factor of two. The distortions were removed from each image, with the exception of the east and west end walls (which had virtually no distortions). In each image, horizontal and vertical markings were used to signify the distorted contour. The undistorted shape was automatically chosen to be a rectangle whose size was roughly that of the distorted shape. After the distortions were estimated and removed, the aspect ratio of each image was adjusted as the images were overlayed, guided by the known chamber dimensions. Variations in global and local lightness/color were corrected for manually. For aesthetic reasons, we identified and digitally removed several modern-day blemishes in background areas. These manipulations were performed in Photoshop.

Shown in Fig. 7, 8 and 9 are the south, north, and west/east walls fully undistorted and seamed together. These undistorted images were then combined with a 3-D model of the burial chamber. Shown in Fig. 10 are several views from the virtual chamber.[3]

6 General Discussion

For several millenia, the remarkable pyramids, temples, statues, and tombs of ancient Egypt have remained as a symbol of this civilization's fascinating history. Over the past few decades these structures have seen significant decay due in part to the ever increasing number of visitors. Digital reconstruction of these structures can help document and preserve these important historical monuments, which in the long run bolsters tourism.

This paper has focused particularly on the task of reconstructing tombs. With respect to the general reconstruction of architecture, these tombs pose new problems and simplify others. At the onset, when photographing in these

[3] A VRML-based virtual chamber and movies of virtual walk-throughs are available at: `www.cs.dartmouth.edu/farid/egypt`.

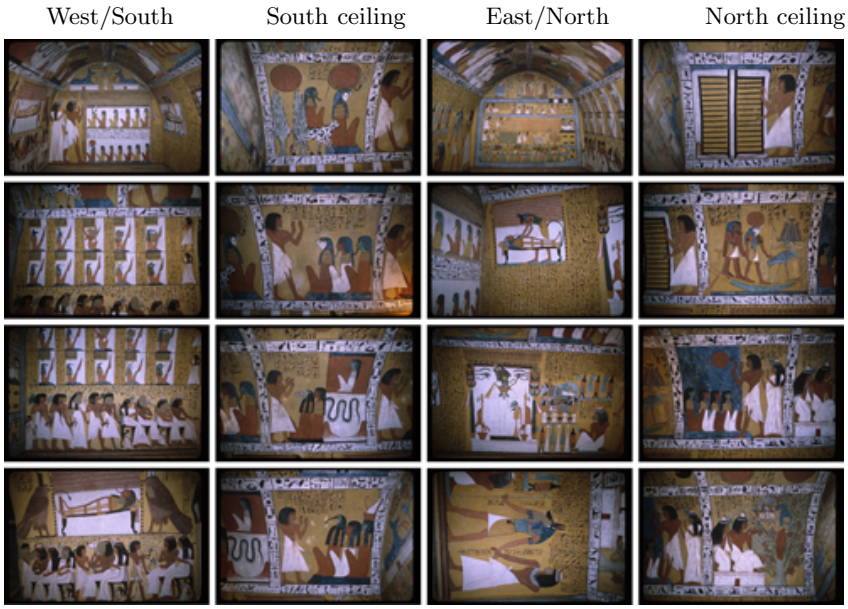

Fig. 6. The sixteen original photographs of Sennedjem's burial chamber.

small tombs (often 2-3 meters wide and tall), it is nearly impossible to avoid significant distortions from the decorated and highly curved ceilings. We have proposed an image-based technique for removing these distortions in the absence of the 3-D structure or intrinsic/extrinsic camera parameters. This technique estimates the distortions by exploiting as fiducial markings the ubiquitous horizontal and vertical hieroglyphic text. This approach should prove to be particularly useful when working from archival photographs. Photographing in these small tombs is further complicated by poor lighting, making it necessary to photograph with a flash. These photographs suffer from the classic problem that the flash does not equally illuminate the scene. The removal of these variations is critical to the creation of a seamless image mosaic. The recent addition of protective glass along the walls has added further complications. In particular, reflections from the flash and from the opposing wall yield substantial artifacts in the photographs. In this regards, we are hopeful that our earlier work on the removal of reflections may prove effective [3]. The relatively simple structure of many tombs greatly simplifies the recovery of their 3-D structure. Many structures are rectangular at the base with a curved ceiling. The curvature of the ceiling can be easily determined from a frontal-parallel view of either end of the structure. Since these structures have been thoroughly studied, the base dimensions are readily available.

Photographing and reconstruction of ancient Egyptian structures poses new and unique problems that this paper has only begun to address. We are

currently working on the reconstruction of several other tombs, and automating many of the manual steps described in this paper.

Acknowledgments

We are most grateful to Samir Farid for many stimulating conversations and suggestions and supplying the photographs of Sennedjem's tomb, and for the generous support from a National Science Foundation CAREER Award (IIS-99-83806), and a departmental National Science Foundation Infrastructure Grant (EIA-98-02068).

References

1. B. Bruyère. *Le Tombe No. 1 de Sennedjem à Deir el Medineh*. Imprimerie De L'Institut Français D'Archeologie Orientale, Cairo, Egypt, 1959.
2. P.E. Debevec, C.J. Taylor, and J. Malik. Modeling and rendering architecture from photographs: a hybrid geometry- and image-based approach. In *SIGGRAPH*, pages 11–20, New Orleans, LA, 1986.
3. H. Farid and E.H. Adelson. Separating reflections from images by use of independent components analysis. *Journal of the Optical Society of America*, 16(9):2136–2145, 1999.
4. M. Hansen, P. Anandan, K. Dana, G. van der Wall, and P. Burt. Real-time scene stabilization and mosaic construction. In *Proceedings of the Second IEEE Workshop on Applications in Computer Vision*, pages 54–62, 1994.
5. R.A. Jarvis. Range from brightness for robotic vision. In *4th International Conference on Robot Vision and Sensory Controls*, pages 165–172, London, England, 1984.
6. G. Maspero. Rapport sur les fouilles et travauxex écutáes en Egypte dans l'hiver de 1885-1886. *Bulletin de l'Institut d'Egypte*, pages 201–208, 1886.
7. W.L. Mitchell and M. Pendlebury. Reconstruction of the Egyptian tomb of Menna using VRML. In *Short paper proceedings of the 3rd UK Virtual Reality Special Interest*, pages 67–73, 1996.
8. H.S. Sawhney and R. Kumar. True multi-image alignment and its application to mosaicing and lens distortion correction. *IEEE Transactions on Pattern Analysis and Machine Intelligence*, 21(3):235–243, 1999.
9. R. Szeliski. Image mosaicing for tele-reality applications. In *Proceedings of the Second IEEE Workshop on Applications in Computer Vision*, pages 44–53, 1994.

Fig. 7. The "unfolded" south wall.

Fig. 8. The "unfolded" north wall.

Fig. 9. The west and east walls.

Fig. 10. Views from the virtual chamber.